Review article

Liqin Tang, Daohong Song*, Shiqi Xia, Shiqiang Xia, Jina Ma, Wenchao Yan, Yi Hu, Jingjun Xu, Daniel Leykam and Zhigang Chen*

Photonic flat-band lattices and unconventional light localization

https://doi.org/10.1515/nanoph-2020-0043
Received January 20, 2020; revised March 3, 2020; accepted March 3, 2020

Abstract: Flat-band systems have attracted considerable interest in different branches of physics in the past decades, providing a flexible platform for studying fundamental phenomena associated with completely dispersionless bands within the whole Brillouin zone. Engineered flat-band structures have now been realized in a variety of systems, in particular, in the field of photonics. Flat-band localization, as an important phenomenon in solid-state physics, is fundamentally interesting in the exploration of exotic ground-state properties of many-body systems. However, direct observation of some flat-band phenomena is highly nontrivial in conventional condensed-matter systems because of intrinsic limitations. In this article, we briefly review recent developments on flat-band localization and the associated phenomena in various photonic lattices, including compact localized states, unconventional line states, and noncontractible loop states. We show that the photonic lattices offer a convenient platform for probing the underlying physics of flat-band systems, which may provide inspiration for exploring the fundamentals and applications of flat-band physics in other structured media from metamaterials to nanophotonic materials.

Keywords: artificial Dirac materials; flat-band states; real-space topology; Kagome and Lieb lattices; super-honeycomb lattices; noncontractible loop states.

1 Introduction

Two-dimensional (2D) photonic systems with flat-bands have attracted increasing interest in recent years [1, 2], inspired by multiband Hubbard models earlier introduced in condensed matter physics [3–5]. A flat-band is a completely dispersionless energy band that extends in the whole Brillouin spectrum [6–9]. As the kinetic energy is completely quenched, which suppresses wave transport, particle interaction becomes dominant, leading to some exotic or unconventional correlated ground states. Such enhanced interaction makes flat-band systems a perfect candidate for investigation of complex many-body quantum states and the physics of strongly correlated systems in the absence of a magnetic field [5, 10–19]. One well-known example is the fractional quantum Hall effect, where the interaction induces nontrivial behavior of the electrons in topological flat-bands [20–22]. Numerous efforts have been made to understand the underlying flat-band physics within the community of ultracold atomic gases [23, 24] and exciton-polariton condensates [25]. It has also been predicated that the flat-band features can support nonlinear compactons [26, 27] and interaction-induced topological phases [28], which open up new avenues for studying the interplay between nonlinearity and spin-orbit coupling phenomena in topological

***Corresponding authors: Daohong Song,** The MOE Key Laboratory of Weak-Light Nonlinear Photonics, TEDA Applied Physics Institute and School of Physics, Nankai University, Tianjin 300457, China; and Collaborative Innovation Center of Extreme Optics, Shanxi University, Taiyuan, Shanxi 030006, China, e-mail: songdaohong@nankai.edu.cn; and
Zhigang Chen, The MOE Key Laboratory of Weak-Light Nonlinear Photonics, TEDA Applied Physics Institute and School of Physics, Nankai University, Tianjin 300457, China; Collaborative Innovation Center of Extreme Optics, Shanxi University, Taiyuan, Shanxi 030006, China; and Department of Physics and Astronomy, San Francisco State University, San Francisco, CA 94132, USA, e-mail: zgchen@nankai.edu.cn. https://orcid.org/0000-0001-7050-9943
Liqin Tang, Shiqi Xia, Jina Ma, Wenchao Yan, Yi Hu and Jingjun Xu: The MOE Key Laboratory of Weak-Light Nonlinear Photonics, TEDA Applied Physics Institute and School of Physics, Nankai University, Tianjin 300457, China; and Collaborative Innovation Center of Extreme Optics, Shanxi University, Taiyuan, Shanxi 030006, China. https://orcid.org/0000-0001-8029-7091 (L. Tang)
Shiqiang Xia: Engineering Laboratory for Optoelectronic Technology and Advanced Manufacturing, Henan Normal University, Xinxiang, Henan 453007, China
Daniel Leykam: Center for Theoretical Physics of Complex Systems, Institute for Basic Science (IBS), Daejeon 34126, Republic of Korea

flat-band systems. Thus far, flat-bands have been realized in a variety of systems including ultracold atoms, various metamaterials, electronic and other realistic materials, and photonic waveguide arrays [29–41]. A detailed account on artificial flat-band systems and related discussions can be found in recent review articles [1, 2] (see, e.g. Ref. [42] for further articles related to flat-band magnetism in frustrated crystals, and Refs. [43, 44] for a review on topological flat bands).

Artificial photonic structures can provide controllable platforms to explore physical phenomena that are difficult to achieve in real materials. In particular, photonic lattices have proven to be extremely effective for investigating fundamental physics in simple optical settings. The underlying physics involved relies on the analogy between the paraxial equation for electromagnetic waves and the Schrödinger equation describing quantum phenomena. Photonic lattices offer exquisite control of initial conditions and allow for monitoring the actual wave functions (including phase). Therefore, it is possible to directly observe wave dynamics using classical light waves in photonic lattices. Over the past two decades, many intriguing fundamental phenomena have been demonstrated in evanescently coupled waveguide arrays created using either femtosecond (fs)-laser writing or optical induction technique, including discrete solitons, dynamical localization, and Anderson localization in disordered lattices [45–53]. These developments have opened up new avenues for the manipulation of light.

Femtosecond laser writing of photonic lattices was first implemented in 2004 for the fabrication of dielectric waveguide arrays [54]. Since then, many successful and fascinating examples of laser-written photonic structures have been realized with this technology. In the fs-laser-writing method, typically a focused laser pulse is sent into bulk fused silica, which creates a localized permanent increase in the refractive index of the material. Consequently, when moving the sample with respect to the writing beam, a longitudinally extended index modification (a waveguide) is created. This fabrication method has the advantage of supporting the generation of compact two-and high-dimensional lattices of nearly arbitrary geometries, leading to the observation of a variety of fundamental phenomena in such lattices.

In Figure 1, we show some typical examples of laser-written and engineered flat-band photonic lattices. Laser-written photonic Lieb lattices [58] were first created by two independent groups (Mukherjee et al. [30] and Vicencio et al. (Figure 1A) [32]) for the observation of *compact localized states* (CLSs). Recently, Hassan et al. reported the experimental realization of novel topological corner states of light in laser-written 2D photonic Kagome lattices (Figure 1B) [55]. Two-dimensional honeycomb-like lattices, known as photonic graphene [59], which have been used to explore photonic Landau levels [60] and Floquet topological insulators [61, 62], have recently been established with engineered micropillar photonic resonators for the demonstration of type-III Dirac cones that combine flat and linear dispersions (Figure 1C) [56]. As another example, losses can be introduced by rapid longitudinal bending of the waveguides or introducing scatters in the laser-writing technique, enabling the realization of non-Hermitian lattice Hamiltonians [63], which leads to the demonstration of PT (parity-time)-symmetric flat-bands (Figure 1D) [57].

In this mini-review, we focus on novel phenomena in optically induced flat-band lattices established in nonlinear crystals. We mainly revisit our recent experimental and theoretical progress in the demonstration of flat-band states and novel light localization in engineered photonic flat-band lattices. In Section 2, we briefly summarize two kinds of flexible approaches based on the optical induction technique to obtain photonic flat-band lattices. In Section 3, we review the numerical method and theory for the calculation and simulation of flat-band light localization in photonic lattices. In subsequent sections, recent experimental work is summarized with respect to the demonstrations of conventional flat-band states – the so-called CLSs in Lieb and Kagome lattices as well as in driven rhombic lattices. Unconventional flat-band localized line states due to the flat-band touching dispersive bands in photonic Lieb and super-honeycomb lattices (sHCLs) are summarized in Section 5. These line states, independent of linear superpositions of conventional bulk CLSs, can be considered as an indirect illustration of the *non-contractible loop states* (NLSs). Furthermore, in Section 6 we discuss two alternative approaches to directly observe NLSs in photonic Kagome lattices: one is to realize the robust boundary modes spanning the whole boundary of a finite lattice, and the other is to achieve direct observation of the NLS in an annular-shaped Kagome lattice, which hosts such a loop state along the toroidal direction. These robust boundary modes and NLSs are direct manifestations of the real-space topology in such flat-band systems. Finally, in Section 7 we summarize our work and present some outlooks for future exploration of the field. This review is not intended to be a comprehensive account of the vast flat-band literature, nor to repeat the published reviews on this subject [1, 2], but it is rather a concise account of the study (mainly from our group) on flat-band phenomena in various photonic lattices.

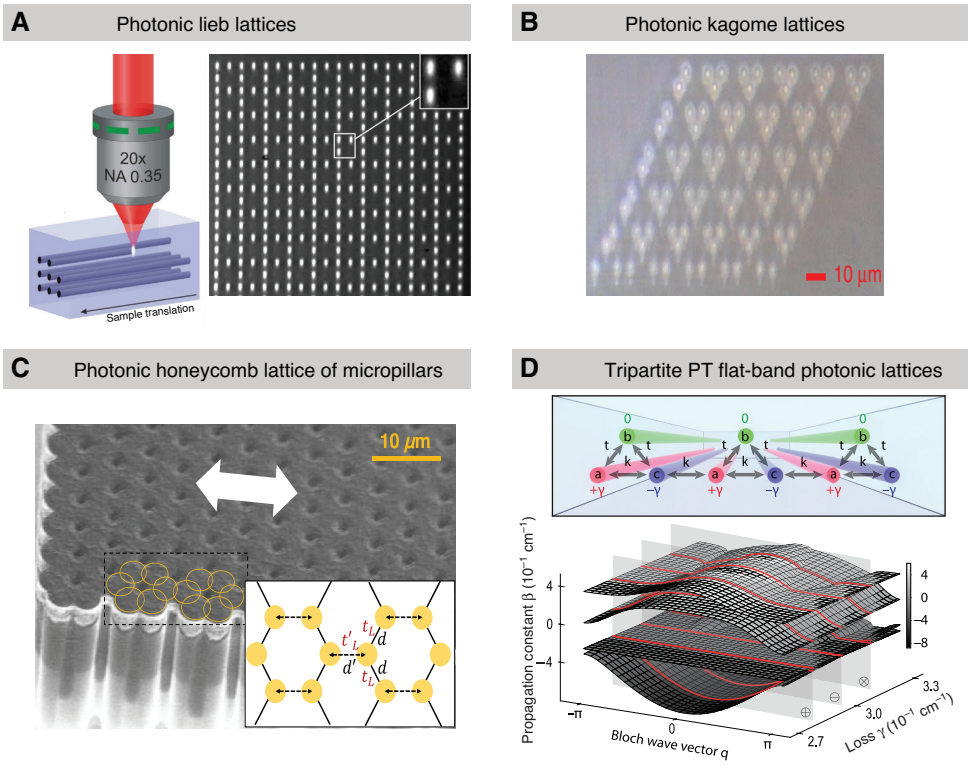

Figure 1: Examples of laser-written and engineered flat-band photonic lattices.
(A) A photonic Lieb lattice established by fs-laser-writing technique for demonstration of flat-band compact localized states [32]. (B) A photonic Kagome lattice established for demonstrating topological corner states exhibiting a remarkable degree of flexibility and control [55]. (C) A photonic honeycomb lattice of micropillars engineered with type-III Dirac cones that combine flat and linear dispersion bands [56]. (D) Schematic of the tripartite PT-symmetric photonic lattice and resulting dispersion relation showing the partially flat band around the exceptional point of the structure [57].

2 Experimental method of lattice induction

Optical induction is a simple yet effective method for the creation of photonic waveguide lattices [45, 46]. The induction technique is based on optically induced nonlinear refractive index change in a bulk nonlinear crystal, somewhat similar to that in the generation of optical spatial solitons (see Ref. [51] for a detailed review). This technique, especially in photorefractive materials, allows the realization of reconfigurable (non-permanent) photonic lattice structures [46, 50, 64–66], in contrast to the fs-laser-writing technique that inscribes structures permanently in silica glass [67, 68]. In what follows, we discuss two main approaches for the realization of photonic lattices using optical induction in photorefractive crystals. The first one uses periodic nondiffracting waves, where the phase and amplitude of multiple interfering plane waves can be modulated to create different 2D periodic lattices. Many of the original studies on optically induced lattices were associated with this method. The other technique, developed more recently, is the site-to-site continuous wave (cw)-laser-writing technique, as shown in Figure 2. Compared with the former method, the latter has the advantage of flexibly establishing lattices with tailored boundaries, as well as aperiodic lattices of arbitrary structures.

2.1 Multiple-beam interference optical induction technique

Multiple-beam interference optical induction was first proposed for the experimental observation of 2D optical discrete solitons in photonic lattices, following the prediction by Efremidis et al. [45]. Soon afterward, this technique was further developed using partially coherent beams featured with the suppression of modulation instability in nonlinear media [69]. Such a mechanism of the optical induction provided an effective way for inducing nonlinear photonic lattices and various reconfigurable photonic structures with defects and surfaces [70], and for the recent demonstrations of photonic graphene lattices

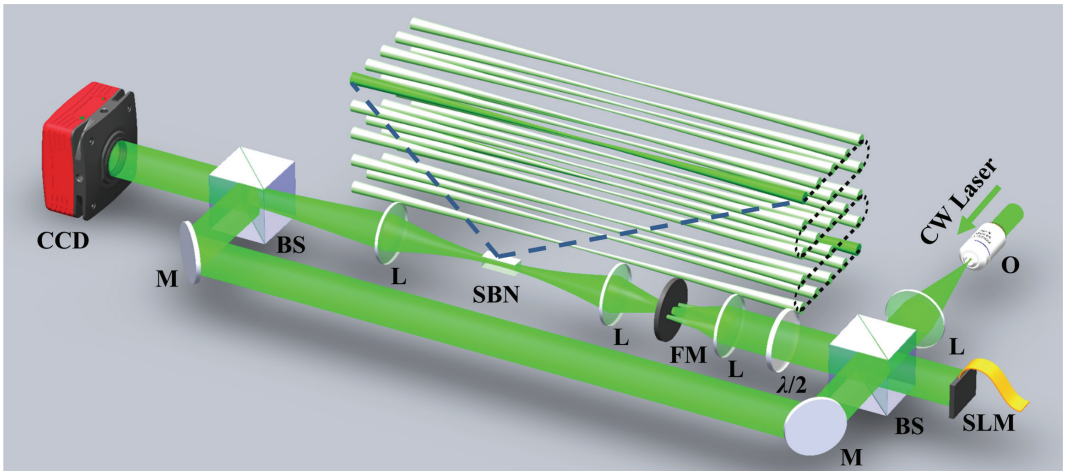

Figure 2: Experimental setup for site-to-site writing of a photonic lattice with a cw laser in a nonlinear photorefractive SBN crystal. SLM, spatial light modulator; BS, beam splitter; FM, Fourier mask; SBN, strontium barium niobate.

for exploring a variety of fundamental phenomena including edge states [69] and pseudospin angular momentum [64, 71, 72].

We now discuss how to fabricate 2D artificial photonic flat-band lattices using the multiple-beam interference optical induction technique in bulk photorefractive materials. In this method, the key point is to create a nondiffracting intensity pattern that can remain invariant throughout the nonlinear crystal by actively suppressing the Talbot effect of the lattice-inducing beams [69]. As such, an amplitude mask and a phase mask for initial phase modulation are typically used in the Fourier plane (momentum space) to achieve different lattice patterns, as done in most of our experiments [73]. Other variations of the method have also been implemented, such as phase control with a specific filter system [74, 75]. The optical induction experimental technique has led to the fabrication of various 2D photonic lattices, from the graphene-like "perfect" honeycomb lattices to MoS_2-like lattices, vortex lattices, and the Kagome lattices. The difference lies in the initial phase/amplitude modulations.

Such interference-based optical induction, however, has limitations for creating some lattices when the spatial spectra of the consisting beams do not reside in a conical ring. A typical example is the Lieb lattice. The Lieb lattice, a 2D analog of the 3D lattice exhibited by perovskites [76], is one of the simplest models of flat-band systems, with a band structure featuring Dirac cones intersected by a flat band. Lieb lattices have now been realized in a variety of settings, ranging from photonic devices [30, 32, 77–81] and electronic systems [40] to ultracold atomic gases [23]. In the photonics community, the linear propagation dynamics of light beam in photonic Lieb waveguide arrays are mostly investigated in fs-laser-written structures [30, 32, 79]. Since the Lieb lattice is not a simple Bravais lattice, it has three sites per unit cell in the edge-centered square structure, and its spectrum does not fit into a ring, as is the case for the honeycomb lattice. Therefore, if one wants to fabricate a Lieb lattice by the multiple-beam interference technique, some necessary means of implementation must be included. In our early experiment [35], a simple yet effective method to solve the above problem was to use two sets of lattices for incoherent superposition. In order to generate a photonic lattice that is invariant along the propagation direction, a quasi-nondiffracting light pattern, normally constructed by the interference of several plane waves, is required. Consequently, superposition of two or more simple optical patterns that are mutually incoherent to each other is necessary, as realized for creating one-dimensional (1D) superlattices [82]. In the experiment for the Lieb case, two sets of lattice beams, namely an "egg-crate" lattice [83] and a square lattice, are used. Note that the intensity maxima of the square pattern exactly fill in the intensity minima of the "egg-crate" pattern. Consequently, the intensity minima form the structure of the Lieb lattice by employing the self-defocusing nonlinearity in a photorefractive SBN (strontium barium niobate) crystal. Such kind of incoherent superposition (ingeniously using an egg-crate lattice) can be widely used in the generation of other superlattices, such as the topological Su-Schrieffer-Heeger lattices [82] in one and two dimensions.

2.2 Site-to-site cw-laser-writing technique

The methods mentioned above are used to fabricate different "unbounded" lattice structures without considering

the lattice termination. However, sometimes we need to prepare some lattice patterns with specially tailored boundaries or edges. Like graphene, different edges support different edge states and have different characteristics. For instance, some flat-band states can only exist in lattices with appropriate boundaries, such as the extended flat-band line states [81, 84–86] discussed in later sections. In order to observe such states, we develop a simple cw-laser-writing technique which can establish finite-sized photonic lattices with desired boundaries. Figure 2 shows a schematic of the experimental setup. An ordinarily polarized quasi-nondiffracting beam from a solid-state laser ($\lambda = 532$ nm) is used to illuminate a spatial light modulator (SLM), which creates a writing beam with reconfigurable input positions. The 4f system guarantees a quasi-nondiffracting zone of the beam as it propagates through the crystal. The technique relies on site-to-site inducing or writing waveguides in a nonlinear photorefractive (SBN) crystal. All the waveguides remain intact during the writing process due to the "memory" effect of the nonlinear photorefractive crystal. Different from the fs-laser-writing technique [67], a lattice written in the bulk crystal is readily reconfigurable, since one can easily erase it with white light and rewrite another lattice in the same crystal. In addition, since the crystal has strong photorefractive nonlinearity, one can st udy nonlinear wave dynamics in such lattices. Apparently, this method is not only limited to creating photonic Lieb lattices but also can be used to flexibly realize some flat-band lattices with virtually arbitrary lattice edges, any ribbon or aperiodic photonic lattices (see Figure 3 for some examples). However, although this method is very flexible, it also has the disadvantage that the period of the lattice cannot be too small (typically around 26 μm or more) due to the limitation of "nondiffracting" region of the writing beam [81], even when the writing beam is a Bessel beam [80].

3 Numerical method and flat-band classification

The evolution of a light beam through a photonic lattice is well described by the following Schrödinger-type equation under the paraxial approximation [46, 50, 51]:

$$i\frac{\partial}{\partial z}\psi(x,y,z)=\left[\frac{-1}{2k_0n_0}\nabla_\perp^2-k_0\Delta n(x,y)\right]\psi(x,y,z), \qquad (1)$$

where ψ corresponds the slowly varying electric field envelop of the probe beam, (x, y) are the transverse dimensions, z represents the longitudinal propagation distance into the photonic lattice, $\nabla_\perp^2$ is the 2D transverse Laplacian operator, n_0 is the unperturbed refractive index of the nonlinear medium, k_0 is the wave number in the vacuum, $\Delta n(x, y)$ represents the local refractive index

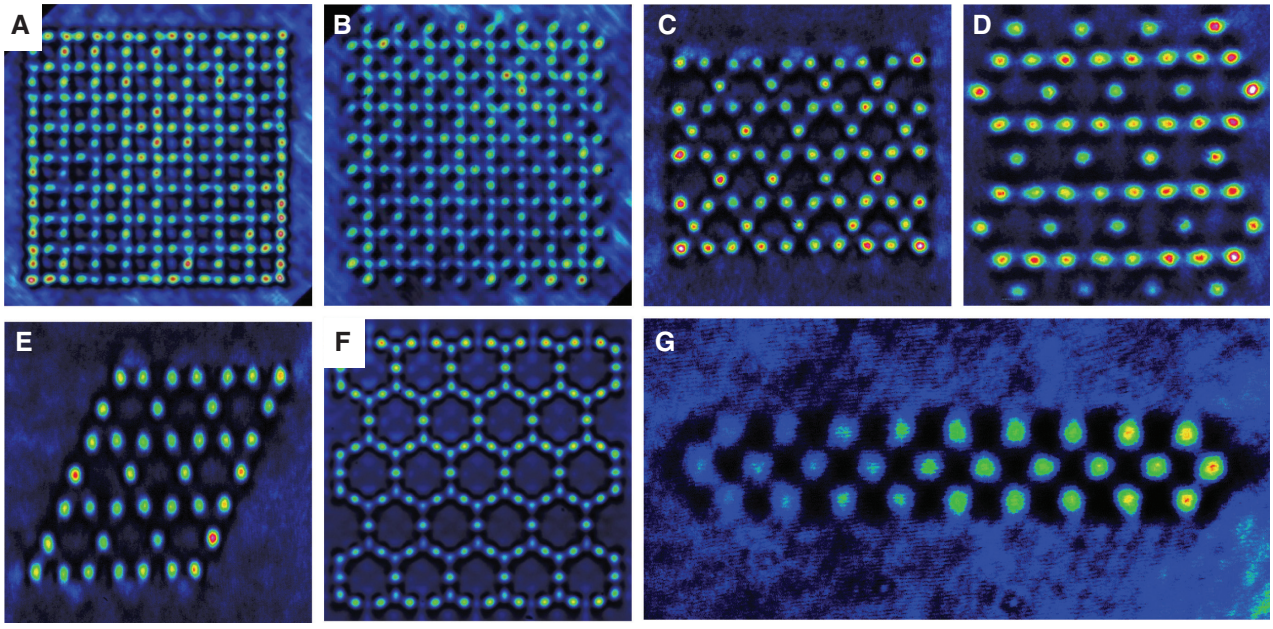

Figure 3: Typical examples of the flat-band photonic lattices created in a nonlinear bulk crystal with the cw-laser-writing technique. (A, B) Lieb [81] lattices with different boundary terminations, (C–E) Kagome lattices with different boundary terminations [86], (F) a super-honeycomb lattice [85], and (G) a "driven" rhombic lattice with an index gradient [84].

change corresponding to a particular 2D photonic lattice under study, with $\Delta n \ll n_0$. Equation (1) has the form of the Schrödinger equation when the replacement is taken as $z \to t$ and $\Delta n \to V$. The localization of flat-band states in lattices requires a stationary potential, implying that the index change Δn in Eq. (1) must be propagation-invariant; that is, $\Delta n(x, y)$ must be z-independent. Experimentally, this corresponds to generation of a nondiffracting lattice-inducing beam pattern as described above.

Under the tight-binding approximation, the above continuous Schrödinger-like equation can be replaced by a discrete equation, considering only the nearest neighbour coupling effect. By Fourier transforming the tight-binding Hamiltonian into the k space, one readily obtains the band structure. A lattice of dispersionless energy band means that there exists at least one complete flat-band in its spectrum, and the corresponding linear Bloch modes are entirely compact localized due to the destructive interference of extended waves. That is, the eigenstate amplitudes strictly vanish except at a finite number of unit cells of the structure. This is particularly interesting because, in this case, waves can stay localized in the continuum. Additionally, these states may be robust against the presence of disorder in the system [87, 88].

Considering the properties of their eigenstates, flat-bands can be classified into three types [2]: "symmetry-protected" flat-bands, "accidental" flat-bands, and "topologically protected" flat-bands. In 1D settings, the CLS can be classified by the integer number U of unit cells they occupy [89]. "Symmetry-protected" chiral flat-bands, first introduced by Shima et al. [90], such as with the cross-stitch lattice ($U = 1$), form an orthogonal set with the simplest CLSs occupying only one unit cell of the lattice. "Accidental" flat-bands can be regarded as the case of $U \geq 2$ with CLSs spanning over more than one unit cell formed by precisely adjusting the system parameters, such as with the sawtooth lattice [34, 91]. In such cases, the band is not always flat, as it only exists in some specific parameter regimes, while, the "topologically protected" flat-bands can be regarded as robust flat-bands, represented by a bipartite system such as the Lieb lattice with two sublattices. Bandcrossing is protected in a sense that it can only be removed by perturbations that also destroy the flatness of the band [92]. Like the protection of the Dirac points of graphene, the mechanism for this stability is topological. Very recently, Rhim and Yang [93] showed that flat-bands can be classified into two distinct classes, singular or nonsingular, based on whether the corresponding Bloch functions exhibit a discontinuity at the crossing points with other bands.

4 Compact localized states in flat-band lattices

The characteristic of flat-band lattices is the existence of the fundamental CLS. The first study of flat-band models started with the work by Sutherland [94]. In his paper, the existence of strictly localized states of a flat-band was demonstrated in a dice lattice. The localized states persist because of local topology even if the lattice periodicity is destroyed. The proposal of using CLSs to name the flat-band eigenmodes originated from the work by Aoki et al. [95].

In 2015, the first experimental demonstrations of stationary and transversely localized flat-band states were performed in photonic Lieb lattices [30, 32]. Such a flat-band in the Lieb lattices is protected by a chiral symmetry, and its intersection with the dispersive bands is said to be protected by real-space topology [77, 92, 96] (the topology of the inter-site couplings rather than their precise strengths, which will be discussed in detail in later sections), which is robust to the coupling disorder [87, 88]. The photonic Lieb lattice was produced early in 2014 by Guzman-Silva et al. [58], but that work focused more on the edge modes generated by stretching the lattice rather than the existence of the flat-band states (or whether the tight-binding condition is satisfied). In contrast, the work published in 2015 [30, 32] reported direct experimental observation of the fundamental flat-band states in photonic lattices, as demonstrated shortly afterward also with optical induced photorefractive lattices [35, 36]. These works attracted wide interest because they prove that waves can stay localized in the continuum, even in the absence of any defect [97], disorder [48], or nonlinearity [46]. Demonstrations of CLSs and a variety of associated phenomena have also been discussed in 1D and 2D lattices, including the Stub [39], sawtooth [34, 91], rhombic [31, 38, 84, 98–103], Kagome [36, 86], super-honeycomb [85, 104], and Lieb [35, 81] lattices, thanks to the advanced techniques that allow for precise flat-band engineering. Figure 4 shows some typical experimental results of CLSs observed in the Lieb, rhombic, and sawtooth lattices fabricated by the fs-laser-writing technique. In the case of the sawtooth lattice, wave localization due to presence of an "accidental" flat-band was observed by fine-tuning the inter-site coupling coefficients [34].

In the tight-binding approximation, the Bloch modes of Lieb lattices are only distributed in three bands: a completely degenerate flat-band centered between two dispersive bands, with all three bands touching at the M points ($k_x = k_y = \pi$) (see Figure 5A) [23, 30, 32, 77, 105]. Similar to honeycomb lattices [61, 66], the intersection

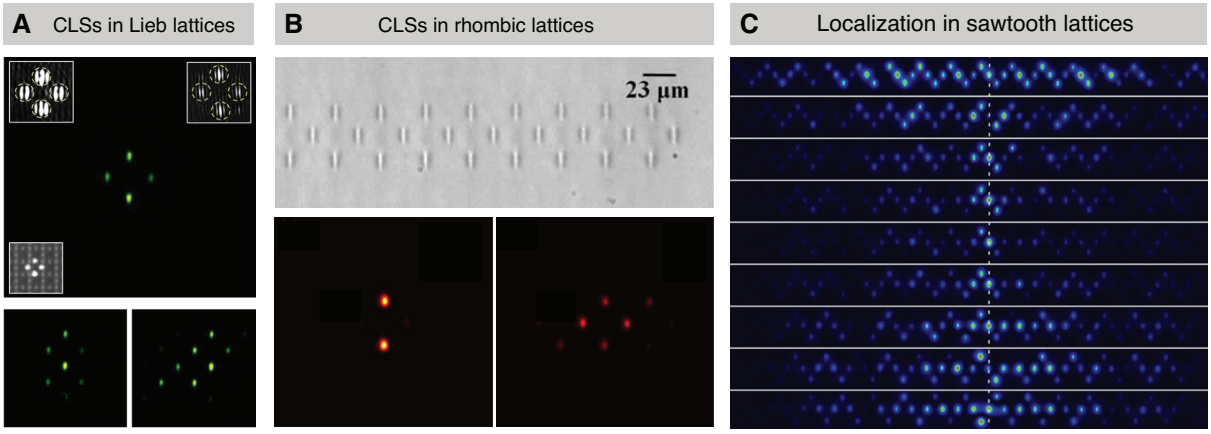

Figure 4: Examples of the compact localized states observed in fs-laser-written flat-band photonic lattices.
(A) The CLSs and their superimposed bound states observed in a Lieb lattice [32]. (B) The CLSs and the equal-phase modes observed in a rhombic lattice [31]. (C) Experimental output intensity for the bulk excitation under different regimes of wave transport in a sawtooth lattice [34].

of the dispersive bands is characterized by a linear dispersion relation in the vicinity of Dirac-like points, leading to intriguing phenomena such as conical diffraction and pseudospin [79, 106]. Furthermore, taking advantage of the superposition of CLSs inherent in the Lieb lattices, flat-band-based text transmission through such 2D perovskite-like photonic structures was demonstrated [35], representing the experimental observation of distortion-free image transmission (Figure 5A) as predicted in Ref. [105]. In those experiments [35], the letter "L" (overlaid by a train of four fundamental modes) was constructed as a probe beam. For comparison, the probe beam with all the pixels being of equal phase is also launched under the same configuration. Obviously, the difference between distorted and undistorted image transmission is evident, as shown in Figure 5A.

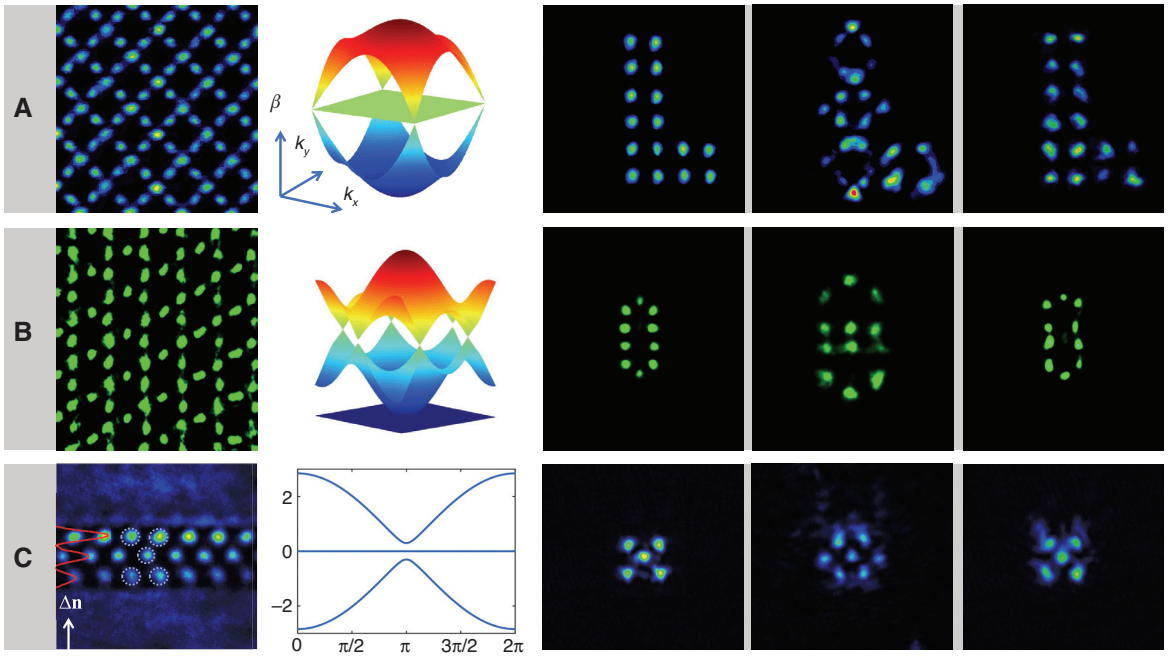

Figure 5: Examples of the compact localized states observed in optically induced flat-band photonic lattices.
Shown are experimental results of (A) linear image propagation through a Lieb photonic lattice [35] and (B) a bound-state transmission in a pyrochlore-like (Kagome) photonic lattice [36]. (C) Experimental observation of a quincunx-shaped CLS which spans over two unit cells in a photonic rhombic lattice [84]. From left to right: the lattice, calculated band structure in the tight-binding approximation, probe beam input, in-phase output, and out-of-phase output.

In addition to the light localization in Lieb lattices, many recent studies have been aimed at understanding the effect of this additional flat-band on various phenomena, including Floquet topological insulators [107], conical diffraction, and integer pseudospin states [79]. The near degeneracy of other bands with zero effective mass is ideal for switching applications and enables novel topological phases with protected edge states in resonance with flat-band states [62, 76, 107].

In the experiments of Zong et al., the first demonstration of CLSs in a Kagome lattice was carried out [36]. In those experiments, they also realized a high-fidelity bound-state transmission through the lattice by judiciously exciting a superposition of flat-band eigenmodes of the Kagome lattice (Figure 5B). Their work may provide inspiration for developing alternative light-trapping and image-transmission schemes in structured photonic materials without engineered disorder or nonlinearity. In addition, one can envisage the possibility for experimental demonstration of predicted novel phenomena such as discrete flat-band solitons and PT-symmetric phase in Kagome photonic lattices [57, 108, 109], and Aharonov-Bohm photonic caging with the implementation of a synthetic gauge field [31, 102, 110].

Flat-band states have also been demonstrated in a rhombic lattice that is robust in the presence of an external driving field (index gradient) along the lattice axis by Mukherjee and Thomson [38]. Recently, Xia et al. [84] demonstrated the existence of CLSs in a driven rhombic lattice ribbon with two distinct refractive index gradients acting as external dc fields. Such CLSs span over two unit cells with a quincunx shape under the action of a driving force. For the first time, the flat-band state of $U=2$ was experimentally realized (see Figure 5C). It is worth mentioning that the external drive added to the ribbon was achieved by modulating the relative intensity of the writing beam. We can see that the flat-band remains flat while the band gap is open, and does not diffract with the opening of the band gap. Comparing the influence of the direction of the index gradient on CLSs, they found that, with a y-gradient set perpendicularly to the ribbon, the undriven CLS turns into a quincunx-shaped CLS spanned over two unit cells (see Figure 5C). In this case, although the flat-band remains, the original flat-band state is no longer maintained, and a new flat-band state is generated that occupies two unit cells. Interestingly, when the index gradient is parallel to the ribbon, Bloch-like oscillation of flat-band states is observed in the momentum space [84].

Apart from the fundamental CLSs observed in the above experiments, there are many theoretical discussions and predictions about the flat-band phenomena under additional symmetry or perturbations. Earlier work of Sutherland reported on the persistence of localized states if the dice lattice periodicity is destroyed [94]. The tunability of the CLSs is another important aspect associated with the flat-band [111]. The robustness of the CLSs to disorder crucially depends on the flat-band feature, for instance, whether the flat-band touches the dispersive bands or not [88]. Bergman et al. discussed about band-touching from real-space topology in frustrated hopping models [92]. Examples of nontrivial and abrupt changes of the wavefunction properties of perturbed flat-band models are the appearance of the flat-band for Landau-Zener Bloch oscillations in the presence of external fields [99], the effect of chiral symmetry-breaking [84] on the flat-band in a partial chiral dimerized Lieb lattice [112], the localization of weakly disordered flat-band states [88], chiral flat-bands with double perturbations, including disorder and synthetic magnetic fields [96], and anomalous topological edge modes in a slowly driven photonic lattice [38, 100].

5 Line states in Lieb and super-honeycomb lattices

The conventional CLSs are compact and localized to a finite area in two dimensions, while the unconventional NLSs are a new type of flat-band eigenstates that are compact and localized in one direction but extended infinitely in the other direction. The existence of such NLSs is related to flat-band crossings with dispersive bands. Moreover, the NLSs are topologically different from the conventional CLSs in real space, as the NLSs cannot be continuously deformed into the conventional CLSs in a torus geometry representing the periodic boundary conditions.

In flat-band systems, one can always find a set of CLSs as degenerate eigenstates, whose energy is the same as that of the flat-band. The full sets of CLSs connected by lattice translation vectors are found to be linearly dependent on each other in certain flat-band systems. As such, the CLS sets are found to be incomplete. Bergman et al. [92] pointed out that in the majority of "frustrated" hopping examples, a flat-band always intersects with other dispersive bands at a number of discrete points in the momentum space. Such band degeneracy is related to the incompleteness of the CLSs in these models. That is to say, there exist some missing states that can complete the flat-band basis. Such missing states are accounted for by noncontractible loops around the torus under periodic boundary conditions (the so-called NLSs). More recently, Rhim et al. theoretically

found that the NLSs are inherent to the singular flat-band, where an immovable singularity exists in the band-crossing of the Bloch wavefunctions [93]. Once the degeneracy at the band-crossing point is lifted, the flat-band becomes dispersive and may acquire a finite Chern number in general. Such real-space topology manifesting via the NLSs of the flat-band is in contradistinction with the recent and widely studied topological features of the Bloch wave functions defined in the momentum space [113, 114].

The NLSs in principle exist in infinite lattices which are experimentally nonfeasible. Recently, NLSs were found to exist even in finite lattices with specially tailored boundaries and satisfy the destructive interference conditions. Such NLSs appear as flat-band line states extended through the entire finite lattice that cannot be obtained by linear superposition of the bulk CLSs. As mentioned above, the band structure of photonic Lieb lattices contains a flat-band intersecting with the two dispersive bands at the Brillion zone (BZ) corners, and the CLSs in Lieb lattices are linearly dependent, which do not form the complete basis of flat-bands. One can find unusually extended flat-band line states, which are compact-localized in one direction but extended in the other direction as shown in Figure 6A. Xia et al. [81] reported the first realization of such unconventional flat-band line states in a finite photonic Lieb lattice with an appropriate termination.

Typical experimental results of the flat-band line states in finite photonic Lieb lattices with the bearded edge are depicted in Figure 6. An input probe beam is shaped into a dotted line pattern with alternatingly opposite phase (see Figure 6B1) and is sent into the cw-laser-written photonic Lieb lattices, as shown in Figure 3B. In the absence of the lattice, the line shape cannot be preserved after free propagation because of the interference between pearls and diffraction of each pearl (see Figure 6B2). In contrast, when such a line beam is launched into the Lieb lattice, its overall intensity pattern is well maintained (Figure 6B3). For direct comparison, the corresponding results for an in-phase line beam (when all pearls are made with equal phase) are presented in Figure 6C1–C3. In the latter case, the line deteriorates as the energy couples to zero-amplitude lattice sites (Figure 6C3). Moreover, a dramatic difference is observed in the *k*-space spectrum between the out-of-phase and in-phase line beams (Figure 6B4 and C4): the spectrum of the out-of-phase line is distributed along the BZ edges where the flat-band touches with the dispersive bands, whereas that of the in-phase one goes to the center of the first BZ. One can see clearly the difference between the out-of-phase beam (intact as unconventional line states) and in-phase beam (strongly distorted). Such unconventional line states cannot be expressed as a linear combination of the previously observed boundary-independent bulk CLSs but rather arise from the nontrivial real-space topology as predicated by the theory [92, 93].

These line states not only represent a novel type of flat-band eigenstates but may also be useful for potential applications such as diffraction-free image transmission. Image transmission based on conventional CLSs has been demonstrated but is limited to a certain necklace-like shape as a superposition of "ring modes" [35]. By combining the features of the CLSs and the new line states, it is possible to realize large-scale image transmission with virtually any pattern extended to lattice boundaries [105]. To illustrate this, the transmission of three different letters based on the combination of the line states and the CLSs is realized with a bearded Lieb lattice [81].

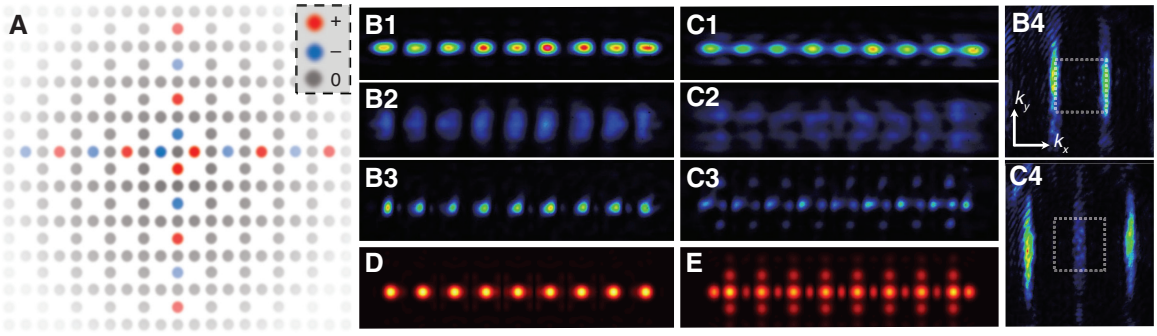

Figure 6: Demonstration of unconventional line states in a photonic Lieb lattice [81].
(A) Schematic illustration of two flat-band NLSs in an infinite Lieb lattice. (B–E) Experimental results of line states in a finite Lieb lattice with bearded edge. (B1) Out-of-phase input line beam. (B2) Out-of-phase output without the lattice. (B3) Out-of-phase output through the lattice. (B4) Measured *k*-space spectrum of (B3), with a dashed square marking the first BZ. (C1–C4) The same as in (B1–B4) but the line beam is in-phase. (D, E) Numerical simulation results showing the out-of-phase line beam remains intact but the in-phase line deteriorates after propagating a long distance through the lattice.

Different from the Lieb lattice, where the flat-band touches the BZ edge, there are also flat-band lattices where the flat-band touching emerges at other high-symmetry points such as the sHCLs. sHCL was first studied more than two decades ago in the context of electronic systems [95, 115]. Recently Dirac cones and conical diffraction in such superlattices were also theoretically investigated [104, 116, 117] in cold atoms and optics, but experimental study is lacking because of the difficulty in constructing such sophisticated lattices. sHCL has five lattice sites (a–e) per unit cell, as shown in Figure 7A, and its tight-binding band structure consists of five bands, including a completely flat-band touching two dispersive conical bands at the center (Γ point) of the first BZ, which resembles the pseudospin-1 Dirac cone in the Lieb lattice. Interestingly, there are also additional graphene-like pseudospin-1/2 Dirac cones at the BZ corners in Figure 7B. Because the flat-band touches the BZ center, there are also NLSs in sHCLs. According to the geometry of sHCLs, there are two different types of line states in finite lattices with specially tailored boundaries, which manifest as the NLSs in infinite flat-band systems: straight line states along the *x*-direction and the zigzag line states along the *y*-direction, as shown in Figure 7C,D. Typical experimental results of the zigzag line states in a cw-laser-written finite sHCL with bearded edges are shown in Figure 7E–H. To excite the zigzag line state, the probe beam is shaped into the zigzag pattern and launched into the lattice vertically (see Figure 7E in which the white rectangle marks the input position). One clearly finds that only the out-of-phase beam can evolve into a flat-band zigzag line state with a localized intensity pattern (Figure 7F3) after exiting the lattice. It is worth mentioning that the zigzag line states realized here do not exist in either the Lieb or the Kagome lattices, which are unique because of the special geometry of sHCLs. More interestingly, the *k*-space spectra of the two line states reside in the higher order BZ and occupy the higher order BZ centers where the flat-band touches the dispersive bands (Figure 7H), which is also different from that in Lieb lattices (for which the band-touching is at the corners of the BZ). In addition, sHCL has a geometrical structure in real space that is different from that of the Lieb lattice. These differences make the distinct properties of the line states in sHCL, e.g. the zigzag line states that are absent in the Lieb lattice. These results again confirm that the line states are related to the flat-band touching the dispersive bands.

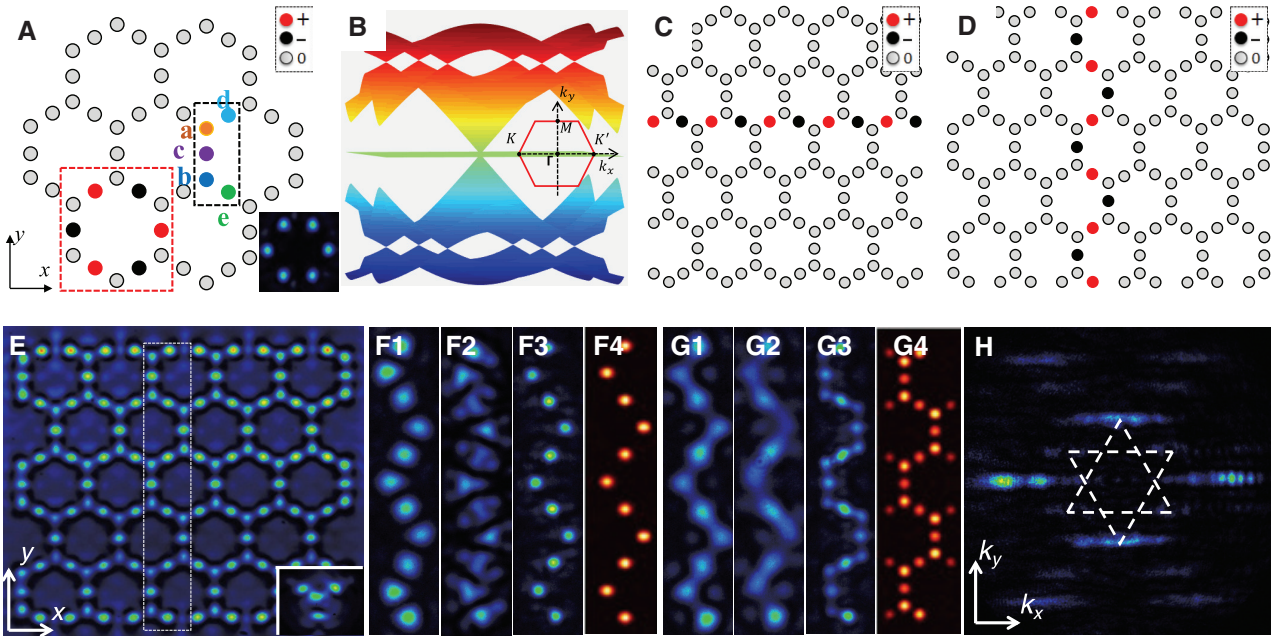

Figure 7: Demonstration of unconventional line states in a finite photonic sHCL with bearded edges [85].
(A) Schematic of sHCL structure consisting of five sites (a–e) shown in dark-dashed square, with a flat-band mode (the CLS) shown in red-dashed square. Sites with zero amplitudes are denoted by gray color, and those with nonzero amplitudes of opposite phase are denoted by red and black colors. (B) Calculated band structure based on the tight-binding model. (C, D) sHCL with two different cutting boundaries that support (C) a "straight" line along x direction and (D) a "zigzag" line along *y*-direction. Red and black colors represent opposite phase.
(E) The cw-laser-written sHCL. The white dashed line marks the position of the probe beam. (F) From left to right: (F1) the input of the out-of-phase probe beam, (F2) output without the lattice, (F3) output through the lattice, and (F4) simulated version of (F3). (G) Setup is as in (F) but with an in-phase probe. (H) Momentum space spectrum of (F3), where the dashed lines outline the first and second BZs.

6 Noncontractible loop states in Kagome lattices

As mentioned above, in finite Lieb or sHCL lattices, the straight or zigzag line states can be preserved under appropriately chosen boundaries. It is natural to ask whether this behavior is universal to all singular flat-band lattices. In fact, this is not always the case. Taking the Kagome lattices as an example, although these lattices have been the focus of numerous studies [24, 52, 105, 118–121], the NLSs originally proposed have never been realized in the Kagome lattices, as it is not feasible to generate an infinite lattice or a torus lattice in experiments. For NLSs in the Kagome lattices, the initial research started with the line states in a truncated system, because Lieb and Kagome photonic lattices are both singular flat-band systems [93]. However, it was found that the line states in finite Kagome lattices are not stable, as their energy can easily dissipate into the bulk [86]. Further theoretical analysis revealed that the line states cannot preserve in truncated Kagome lattices, as a straight-line state cannot be the flat-band eigenmode regardless of the lattice edges, in sharp contrast to the case of Lieb lattices [81].

The experiments by Ma et al. [86] tackled the above problem in two ways. On one hand, they realized the robust boundary modes (RBMs) spanning the whole boundary of the finite lattice, as proposed already in Ref. [93]. The boundary modes arising from the NLSs are robust against perturbation and even possess the self-healing feature during propagation due to bulk-edge correspondence. On the other hand, a torus geometry with periodicities is difficult to be realized in real systems, but one can still preserve the periodicity at least along one direction by using a lattice with an annular (also known as Corbino) geometry. So they fabricated a Corbino-geometry Kagome lattice, and thereby directly observed the NLSs. We note that the Corbino geometry has well-known applications in physics [122–124], such as in the design of graphene heterostructures for detecting fractional quantum Hall states or superconducting waveguides for illustrating circuit quantum electrodynamics.

In Figure 8, the two alternative approaches are shown to reveal the NLSs. Two NLSs are shown in Figure 8A in an infinite Kagome photonic lattice and in Figure 8B on a torus. An RBM can be considered as a combination of the NLSs by cutting the torus in both toroidal and poloidal directions [93]. They create a space with four sides open as if it was a torus generated by truncation. If there are two pairs of NLSs on the torus (one in toroidal and the other in poloidal directions), then by cutting the torus along these directions one can expand it into a finite-sized lattice with four sides open. Then the state existing at the edge of finite size will be the superposition state of the four NLSs (Figure 8C). To observe this boundary mode, an input probe beam is shaped into a necklace of parallelogram shape with opposite phase. When such a probe beam is launched into the lattice boundary, we see clearly that the probe beam is preserved after passing through the lattice (Figure 8E1). The energy of the boundary mode couples into other sites out of the loop (Figure 8E2) if the neighboring sites are in-phase. As such, Kagome lattices with desired "cutting" edges can support RBMs, as an indirect illustration of the NLSs due to bulk-edge correspondence. Such RBMs also can be preserved during propagation in case of superposition with other modes, and possess "self-healing" features against perturbation in either the initial phase or amplitude [86].

Another more direct method to demonstrate NLSs is also shown in Figure 8, which is light localization for the NLSs in the Corbino-shaped photonic Kagome lattice. As illustrated in Figure 8D, with this lattice geometry one can realize the NLS along the toroidal direction, akin to an infinite system in one dimension. For this geometry, the distances between B and C sublattices are equivalent over each ring but increase with the ring diameter; the distances between A and B (or C) sublattices are also equal but these distances within and outside the ring are not dependent. Such a lattice is generated with site-by-site laser writing in a nonlinear crystal, and a typical written lattice is shown in Figure 8F1. Then, a ring-shaped necklace pattern under out-of-phase condition is launched to excite the NLS depicted in Figure 8D. The corresponding experimental results are shown in Figure 8F2, where one can clearly see that the necklace beam remains intact after 10 mm of propagation, as also verified by numerical simulations to even longer propagation distances (Figure 8F3,F4). If the input necklace beam does not have the required alternating phase, it is strongly distorted during propagation since such an input cannot evolve into the NLS. Therefore, these results represent the first demonstration of the NLS originally proposed for the infinite system in Kagome lattices as a direct manifestation of the real-space topology [86, 92, 93].

7 Summary and outlook

We have presented a brief overview of the recent experimental advances of light localization in 1D and 2D engineered flat-band photonic lattices, with an emphasis on

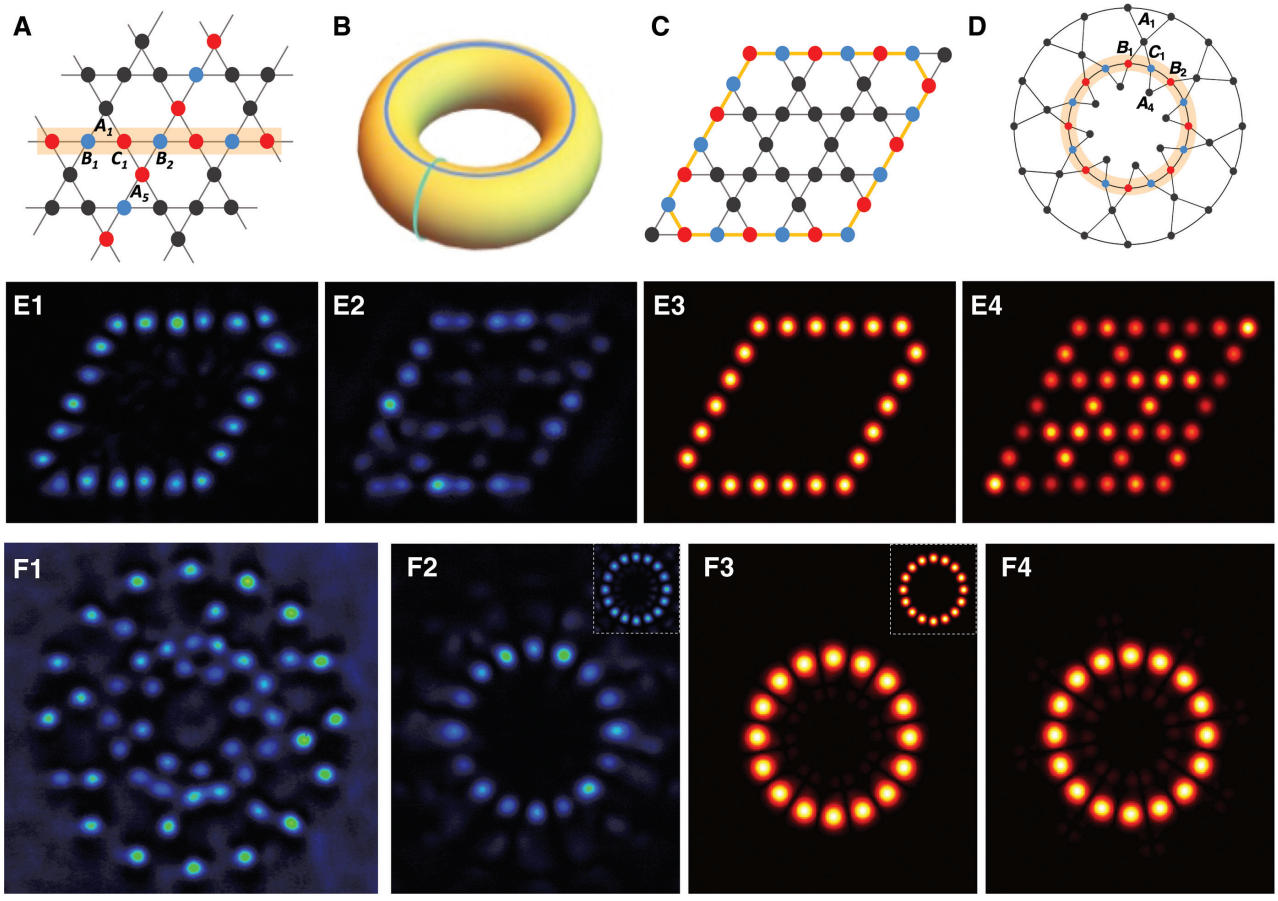

Figure 8: Demonstration of unconventional loop states in a photonic Kagome lattice [86].
(A) Illustration of two NLSs in an infinitely extended Kagome lattice. (B) Illustration of two NLSs winding around a torus, mimicking the 2D infinite lattice. (C) An RBM (orange loop) in a finite Kagome lattice with flat cutting edges. (D) Schematic diagram of a Corbino-shaped Kagome lattice, where the NLS is illustrated by the orange circle. In all figures, black sites are of zero amplitude, while the blue and red ones distinguish nonzero sites with opposite phases. (E) From left to right: (E1, E2) Experimental results of the RBM under out-of-phase and in-phase condition; (E3, E4) Simulation result corresponding to (E1, E2) but for a much longer propagation distance (40 mm). (F) Experimental realization of the Corbino-geometry lattice (F1) corresponding to (D), along with demonstration of the NLS in experiment (F2) and simulations after propagation distance of 10 mm (F3) and 40 mm (F4) under out-of-phase excitation condition. Insets are from input ring necklace of the probe beam.

the optical induction technique and unconventional flat-band states. Using optical induction, we have designed and realized photonic lattices with a variety of shapes and boundaries, such as Lieb lattices, Kagome lattices, super-honeycomb lattices, and rhombic lattices. The fine-tuned photonic structures can be established with the adjustment of lattice period, intensity and phase of the writing beam, and nonlinearity. Based on these flat-band microstructured photonic platforms, we have demonstrated a variety of linearly localized states, such as the fundamental CLSs and the unconventional line states. The concept and techniques presented here could be developed for applications in other structured photonic media, such as photonic crystals and photonic crystal fibers. For example, such schemes could be used to make optical fibers with particular modal properties, or microscopic optical cavities if propagation in the third dimension can be blocked in a convincing way.

Before concluding, we briefly comment on a few notable directions related to flat-band phenomena pursued in other platforms. For instance, in flat-band topology, topological corner states have been realized in photonic Kagome lattices by El Hassan's group [55]. This kind of corner modes relies on crystalline symmetries [125–127] and can be viewed as a variant of crystalline topological insulators [128]. Such simple and convenient means of implementation, in contrast to the much more complex designs with helical optical waveguides [62], drastically enhance the prospects of incorporating these ideas in photonic technological devices. Similar

corner modes have also been explored in acoustic metamaterials [129, 130] and microwave circuits [131]. The report by Lim et al. [132] demonstrated that continuous transformations between Lieb and Kagome lattices are accompanied by the motion of Dirac point degeneracies through the Brilllouin zone. The successful implementation of 2D photonic Moiré lattices by Ye's group [133] made it possible to realize the exciting characteristics of the "magic" twist angles (not merely in the field of light localization), and the existence of flat-bands at certain angles is the physical and fundamental physical origin of Mott insulators [16–18]. Moiré lattices may manifest as an almost arbitrary geometry that is consistent with the crystallographic symmetry groups of the sublattices, which provide a powerful tool for controlling the flow of light. Structured microcavities forming lattices for exciton-polaritons have been used to observe nonlinear localized modes in flat-bands [134] and the generation of flat-bands using strain [135]. In contrast to the above platforms, circuit quantum electrodynamics, which is not limited to planar Euclidean lattice geometries, was recently used to realize a variety of lattices including flat-band lattices on the hyperbolic space [123].

In summary, the study of artificial photonic flat-band lattices and flat-band states has provided and will continue to provide insights into understanding fundamental concepts and phenomena in interdisciplinary areas such as condensed matter physics, materials science, cold atoms, metamaterials, and photonics, which may also lead to new techniques to control the flow of light and to develop novel photonic devices.

Acknowledgments: We thank S. Flach, A. Andreanov, J. W. Rhim, B. J. Yang, and R. A. Vicencio for helpful discussions and assistance, and all our co-workers over the years on the review topic. This work was supported by the National key R&D Program of China under Grant (No. 2017YFA0303800), the National Natural Science Foundation (91750204, 11922408, 11674180, 11704102), the PCSIRT (IRT0149), and the 111 Project (No. B07013) in China, and by the Institute for Basic Science in Korea (IBS-R024-Y1).

References

[1] Leykam D, Andreanov A, Flach S. Artificial flat band systems: from lattice models to experiments. Adv Phys X 2018;3:1473052.
[2] Leykam D, Flach S. Perspective: photonic flatbands. APL Photon 2018;3:070901–16.
[3] Mielke A. Ferromagnetism in the Hubbard model on line graphs and further considerations. J Phys Math Gen 1991;24:3311–21.
[4] Tasaki H. Hubbard model and the origin of ferromagnetism. Eur Phys JB 2008;64:365–72.
[5] Lieb EH. Two theorems on the Hubbard model. Phys Rev Lett 1989;62:1201–4.
[6] Moessner R, Chalker JT. Low-temperature properties of classical geometrically frustrated antiferromagnets. Phys Rev B 1998;58:12049–62.
[7] Harris MJ, Bramwell ST, McMorrow DF, Zeiske T, Godfrey KW. Geometrical frustration in the ferromagnetic pyrochlore $HO_2Ti_2O_7$. Phys Rev Lett 1997;79:2554–7.
[8] Ramirez AP. Strongly geometrically frustrated magnets. Annu Rev Mater Sci 1994;24:453–80.
[9] Huse DA, Rutenberg AD. Classical antiferromagnets on the Kagomé lattice. Phys Rev B 1992;45:7536–9.
[10] Wu C, Bergman D, Balents L, Das Sarma S. Flat bands and Wigner crystallization in the honeycomb optical lattice. Phys Rev Lett 2007;99:070401.
[11] Liu Z, Bergholtz EJ, Fan H, Läuchli AM. Fractional Chern insulators in topological flat bands with higher Chern number. Phys Rev Lett 2012;109:186805.
[12] Möller G, Cooper NR. Correlated phases of Bosons in the flat lowest band of the dice lattice. Phys Rev Lett 2012;108:045306.
[13] Trescher M, Bergholtz EJ. Flat bands with higher Chern number in pyrochlore slabs. Phys Rev B 2012;86:241111.
[14] Weeks C, Franz M. Flat bands with nontrivial topology in three dimensions. Phys Rev B 2012;85:041104.
[15] Liu Z, Wang Z-F, Mei J-W, Wu Y-S, Liu F. Flat Chern band in a two-dimensional organometallic framework. Phys Rev Lett 2013;110:106804.
[16] Cao Y, Fatemi V, Demir A, et al. Correlated insulator behaviour at half-filling in magic-angle graphene superlattices. Nature 2018;556:80–4.
[17] Cao Y, Fatemi V, Fang S, et al. Unconventional superconductivity in magic-angle graphene superlattices. Nature 2018;556:43–50.
[18] Xu C, Balents L. Topological superconductivity in twisted multilayer graphene. Phys Rev Lett 2018;121:087001.
[19] Yuan NFQ, Fu L. Model for the metal-insulator transition in graphene superlattices and beyond. Phys Rev B 2018;98:045103.
[20] Tang E, Mei J-W, Wen X-G. High-temperature fractional quantum Hall states. Phys Rev Lett 2011;106:236802.
[21] Sun K, Gu Z, Katsura H, Das Sarma S. Nearly flatbands with nontrivial topology. Phys Rev Lett 2011;106:236803.
[22] Neupert T, Santos L, Chamon C, Mudry C. Fractional quantum Hall states at zero magnetic field. Phys Rev Lett 2011;106:236804.
[23] Taie S, Ozawa H, Ichinose T, Nishio T, Nakajima S, Takahashi Y. Coherent driving and freezing of bosonic matter wave in an optical Lieb lattice. Sci Adv 2015;1:e1500854.
[24] Jo G-B, Guzman J, Thomas CK, Hosur P, Vishwanath A, Stamper-Kurn DM. Ultracold atoms in a tunable optical Kagome lattice. Phys Rev Lett 2012;108:045305.
[25] Masumoto N, Kim NY, Byrnes T, et al. Exciton–polariton condensates with flat bands in a two-dimensional Kagome lattice. New J Phys 2012;14:065002.
[26] López-González D, Molina MI. Linear and nonlinear compact modes in quasi-one-dimensional flatband systems. Phys Rev A 2016;93:043847.
[27] Gligorić G, Maluckov A, Hadžievski L, Flach S, Malomed BA. Nonlinear localized flat-band modes with spin-orbit coupling. Phys Rev B 2016;94:144302.

[28] Di Liberto M, Hemmerich A, Morais Smith C. Topological Varma superfluid in optical lattices. Phys Rev Lett 2016;117:163001.
[29] Nakata Y, Okada T, Nakanishi T, Kitano M. Observation of flat band for terahertz spoof plasmons in a metallic Kagome lattice. Phys Rev B 2012;85:205128.
[30] Mukherjee S, Spracklen A, Choudhury D, et al. Observation of a localized flat-band state in a photonic Lieb lattice. Phys Rev Lett 2015;114:245504.
[31] Mukherjee S, Thomson RR. Observation of localized flat-band modes in a quasi-one-dimensional photonic rhombic lattice. Opt Lett 2015;40:5443–6.
[32] Vicencio RA, Cantillano C, Morales-Inostroza L, et al. Observation of localized states in Lieb photonic lattices. Phys Rev Lett 2015;114:245503.
[33] Kajiwara S, Urade Y, Nakata Y, Nakanishi T, Kitano M. Observation of a nonradiative flat band for spoof surface plasmons in a metallic Lieb lattice. Phys Rev B 2016;93:075126.
[34] Weimann S, Morales-Inostroza L, Real B, Cantillano C, Szameit A, Vicencio RA. Transport in sawtooth photonic lattices. Opt Lett 2016;41:2414–7.
[35] Xia S, Hu Y, Song D, Zong Y, Tang L, Chen Z. Demonstration of flat-band image transmission in optically induced Lieb photonic lattices. Opt Lett 2016;41:1435–8.
[36] Zong Y, Xia S, Tang L, et al. Observation of localized flat-band states in Kagome photonic lattices. Opt Express 2016;24:8877–85.
[37] Drost R, Ojanen T, Harju A, Liljeroth P. Topological states in engineered atomic lattices. Nat Phys 2017;13:668–71.
[38] Mukherjee S, Thomson RR. Observation of robust flat-band localization in driven photonic rhombic lattices. Opt Lett 2017;42:2243–6.
[39] Real B, Cantillano C, López-González D, et al. Flat-band light dynamics in Stub photonic lattices. Sci Rep 2017;7:15085.
[40] Slot MR, Gardenier TS, Jacobse PH, et al. Experimental realization and characterization of an electronic Lieb lattice. Nat Phys 2017;13:672–6.
[41] Lin Z, Choi J-H, Zhang Q, et al. Flatbands and emergent ferromagnetic ordering in Fe_3Sn_2 Kagome lattices. Phys Rev Lett 2018;121:096401.
[42] Derzhko O, Richter J, Maksymenko M. Strongly correlated flat-band systems: the route from Heisenberg spins to Hubbard electrons. Int J Mod Phys B 2015;29:1530007.
[43] Parameswaran SA, Roy R, Sondhi SL. Fractional quantum Hall physics in topological flat bands. CR Phys 2013;14:816–39.
[44] Bergholtz EJ, Liu Z. Topological flat band models and fractional Chern insulators. Int J Mod Phys B 2013;27:1330017.
[45] Efremidis NK, Sears S, Christodoulides DN, Fleischer JW, Segev M. Discrete solitons in photorefractive optically induced photonic lattices. Phys Rev E 2002;66:046602.
[46] Fleischer JW, Segev M, Efremidis NK, Christodoulides DN. Observation of two-dimensional discrete solitons in optically induced nonlinear photonic lattices. Nature 2003;422:147–50.
[47] Longhi S, Marangoni M, Lobino M, et al. Observation of dynamic localization in periodically curved waveguide arrays. Phys Rev Lett 2006;96:243901.
[48] Schwartz T, Bartal G, Fishman S, Segev M. Transport and Anderson localization in disordered two-dimensional photonic lattices. Nature 2007;446:52–5.
[49] Lahini Y, Avidan A, Pozzi F, et al. Anderson localization and nonlinearity in one-dimensional disordered photonic lattices. Phys Rev Lett 2008;100:013906.
[50] Lederer F, Stegeman GI, Christodoulides DN, Assanto G, Segev M, Silberberg Y. Discrete solitons in optics. Phys Rep 2008;463:1–126.
[51] Chen Z, Segev M, Christodoulides DN. Optical spatial solitons: historical overview and recent advances. Rep Prog Phys 2012;75:086401.
[52] Nixon M, Ronen E, Friesem AA, Davidson N. Observing geometric frustration with thousands of coupled lasers. Phys Rev Lett 2013;110:184102.
[53] Segev M, Silberberg Y, Christodoulides DN. Anderson localization of light. Nat Photon 2013;7:197–204.
[54] Pertsch T, Peschel U, Lederer F, et al. Discrete diffraction in two-dimensional arrays of coupled waveguides in silica. Opt Lett 2004;29:468–70.
[55] El Hassan A, Kunst FK, Moritz A, Andler G, Bergholtz EJ, Bourennane M. Corner states of light in photonic waveguides. Nat Photon 2019;13:697–700.
[56] Milićević M, Montambaux G, Ozawa T, et al. Type-III and tilted Dirac cones emerging from flat bands in photonic orbital graphene. Phys Rev X 2019;9:031010.
[57] Biesenthal T, Kremer M, Heinrich M, Szameit A. Experimental realization of PT-symmetric flat bands. Phys Rev Lett 2019;123:183601.
[58] Guzmán-Silva D, Mejía-Cortés C, Bandres M, et al. Experimental observation of bulk and edge transport in photonic Lieb lattices. New J Phys 2014;16:063601.
[59] Plotnik Y, Rechtsman MC, Song D, et al. Observation of unconventional edge states in 'photonic graphene'. Nat Mater 2014;13:57–62.
[60] Rechtsman MC, Zeuner JM, Tunnermann A, Nolte S, Segev M, Szameit A. Strain-induced pseudomagnetic field and photonic Landau levels in dielectric structures. Nat Photon 2012;7:153–8.
[61] Rechtsman MC, Plotnik Y, Zeuner JM, et al. Topological creation and destruction of edge states in photonic graphene. Phys Rev Lett 2013;111:103901.
[62] Rechtsman MC, Zeuner JM, Plotnik Y, et al. Photonic Floquet topological insulators. Nature 2013;496:196–200.
[63] Zeuner JM, Rechtsman MC, Plotnik Y, et al. Observation of a topological transition in the bulk of a non-Hermitian system. Phys Rev Lett 2015;115:040402.
[64] Song D, Paltoglou V, Liu S, et al. Unveiling pseudospin and angular momentum in photonic graphene. Nat Commun 2015;6:6272.
[65] Song D, Lou C, Tang L, Ye Z, Xu J, Chen Z. Experiments on linear and nonlinear localization of optical vortices in optically induced photonic lattices. Int J Opt 2012;2012:1–10.
[66] Peleg O, Bartal G, Freedman B, Manela O, Segev M, Christodoulides DN. Conical diffraction and gap solitons in honeycomb photonic lattices. Phys Rev Lett 2007;98:103901.
[67] Szameit A, Burghoff J, Pertsch T, Nolte S, Tünnermann A, Lederer F. Two-dimensional soliton in cubic fs laser written waveguide arrays in fused silica. Opt Express 2006;14:6055–62.
[68] Szameit A, Blömer D, Burghoff J, et al. Discrete nonlinear localization in femtosecond laser written waveguides in fused silica. Opt Express 2005;13:10552–7.
[69] Martin H, Eugenieva ED, Chen Z, Christodoulides DN. Discrete solitons and soliton-induced dislocations in partially coherent photonic lattices. Phys Rev Lett 2004;92:123902.
[70] Chen Z, Segev M, Christodoulides DN. Experiments on partially coherent photorefractive solitons. J Opt A: Pure Appl Opt 2003;5:S389–97.

[71] Song D, Leykam D, Su J, et al. Valley vortex states and degeneracy lifting via photonic higher-band excitation. Phys Rev Lett 2019;122:123903.
[72] Song D, Liu S, Paltoglou V, et al. Controlled generation of pseudospin-mediated vortices in photonic graphene. 2D Mater 2015;2:034007.
[73] Gao Y, Song D, Chu S, Chen Z. Artificial graphene and related photonic lattices generated with a simple method. IEEE Photon J 2014;6:1–6.
[74] Boguslawski M, Rose P, Denz C. Increasing the structural variety of discrete nondiffracting wave fields. Phys Rev A 2011;84:013832.
[75] Boguslawski M, Rose P, Denz C. Nondiffracting Kagome lattice. Appl Phys Lett 2011;98:061111.
[76] Weeks C, Franz M. Topological insulators on the Lieb and perovskite lattices. Phys Rev B 2010;82:085310.
[77] Shen R, Shao LB, Wang B, Xing DY. Single Dirac cone with a flat band touching on line-centered-square optical lattices. Phys Rev B 2010;81:041410(R).
[78] Goldman N, Urban DF, Bercioux D. Topological phases for fermionic cold atoms on the Lieb lattice. Phys Rev A 2011;83:063601.
[79] Diebel F, Leykam D, Kroesen S, Denz C, Desyatnikov AS. Conical diffraction and composite Lieb Bosons in photonic lattices. Phys Rev Lett 2016;116:183902.
[80] Travkin E, Diebel F, Denz C. Compact flat band states in optically induced flatland photonic lattices. Appl Phys Lett 2017;111:011104.
[81] Xia S, Ramachandran A, Xia S, et al. Unconventional flat-band line states in photonic Lieb lattices. Phys Rev Lett 2018;121:263902.
[82] Malkova N, Hromada I, Wang X, Bryant G, Chen Z. Observation of optical Shockley-like surface states in photonic superlattices. Opt Lett 2009;34:1633–5.
[83] Zhang P, Liu S, Lou C, et al. Incomplete Brillouin-zone spectra and controlled Bragg reflection with ionic-type photonic lattices. Phys Rev A 2010;81:041801(R).
[84] Xia S, Danieli C, Yan W, et al. Observation of quincunx-shaped and dipole-like flatband states in photonic rhombic lattices without band-touching. APL Photon 2020;5:016107.
[85] Yan W, Zhong H, Song D, et al. Flatband line states in photonic super-honeycomb lattices. 2019;arXiv:1912.12657 [e-print].
[86] Ma J, Rhim J-W, Tang L, et al. Realization of robust boundary modes and non-contractible loop states in photonic Kagome lattices. 2019;arXiv:1911.00848 [e-print].
[87] Leykam D, Flach S, Bahat-Treidel O, Desyatnikov AS. Flat band states: disorder and nonlinearity. Phys Rev B 2013;88:224203.
[88] Leykam D, Bodyfelt JD, Desyatnikov AS, Flach S. Localization of weakly disordered flat band states. Eur Phys J B 2017;90:1–12.
[89] Flach S, Leykam D, Bodyfelt JD, Matthies P, Desyatnikov AS. Detangling flat bands into Fano lattices. EPL Europhys Lett 2014;105:30001.
[90] Strange JH, Rahman M, Smith EG. Characterization of porous solids by NMR. Phys Rev Lett 1993;71:3589–91.
[91] Johansson M, Naether U, Vicencio RA. Compactification tuning for nonlinear localized modes in sawtooth lattices. Phys Rev E 2015;92:032912.
[92] Bergman DL, Wu C, Balents L. Band touching from real-space topology in frustrated hopping models. Phys Rev B 2008;78:125104.
[93] Rhim J-W, Yang B-J. Classification of flat bands according to the band-crossing singularity of Bloch wave functions. Phys Rev B 2019;99:045107.
[94] Sutherland B. Localization of electronic wave functions due to local topology. Phys Rev B 1986;34:5208–11.
[95] Aoki H, Ando M, Matsumura H. Hofstadter butterflies for flat bands. Phys Rev B 1996;54:R17296–9.
[96] Ramachandran A, Andreanov A, Flach S. Chiral flat bands: existence, engineering, and stability. Phys Rev B 2017;96:161104.
[97] Makasyuk I, Chen Z, Yang J. Band-gap guidance in optically induced photonic lattices with a negative defect. Phys Rev Lett 2006;96:223903.
[98] Longhi S. Aharonov-Bohm photonic cages in waveguide and coupled resonator lattices by synthetic magnetic fields. Opt Lett 2014;39:5892–5.
[99] Khomeriki R, Flach S. Landau-Zener bloch oscillations with perturbed flat bands. Phys Rev Lett 2016;116:245301.
[100] Mukherjee S, Spracklen A, Valiente M, et al. Experimental observation of anomalous topological edge modes in a slowly driven photonic lattice. Nat Commun 2017;8:13918.
[101] Kremer M, Petrides I, Meyer E, Heinrich M, Zilberberg O, Szameit A. Non-quantized square-root topological insulators: a realization in photonic Aharonov-Bohm cages. Nat Commun 2020;11:907.
[102] Mukherjee S, Di Liberto M, Öhberg P, Thomson RR, Goldman N. Experimental observation of Aharonov-Bohm cages in photonic lattices. Phys Rev Lett 2018;121:075502.
[103] Longhi S. Photonic flat-band laser. Opt Lett 2019;44:287–90.
[104] Zhong H, Zhang Y, Zhu Y, et al. Transport properties in the photonic super-honeycomb lattice – a hybrid fermionic and bosonic system. Ann Phys 2017;529:1600258.
[105] Vicencio RA, Mejia-Cortes C. Diffraction-free image transmission in Kagome photonic lattices. J Opt UK 2014;16:015706.
[106] Leykam D, Bahat-Treidel O, Desyatnikov AS. Pseudospin and nonlinear conical diffraction in Lieb lattices. Phys Rev A 2012;86:031805.
[107] Bandres MA, Rechtsman MC, Szameit A, Segev M. Lieb photonic topological insulator. In: 2014 Conference on lasers and electro-optics (CLEO)-laser science to photonic applications. IEEE, 2014:1–2.
[108] Vicencio RA, Johansson M. Discrete flat-band solitons in the kagome lattice. Phys Rev A 2013;87:061803(R).
[109] Chern G-W, Saxena A. PT-symmetric phase in Kagome-based photonic lattices. Opt Lett 2015;40:5806–9.
[110] Zhang P, Gallardo D, Liu S, et al. Vortex degeneracy lifting and Aharonov-Bohm-like interference in deformed photonic graphene. Opt Lett 2017;42:915–8.
[111] Nandy A, Chakrabarti A. Engineering slow light and mode crossover in a fractal-Kagome waveguide network. Phys Rev A 2016;93:013807.
[112] Poli C, Schomerus H, Bellec M, Kuhl U, Mortessagne F. Partial chiral symmetry-breaking as a route to spectrally isolated topological defect states in two-dimensional artificial materials. 2D Mater 2017;4:025008.
[113] Lu L, Joannopoulos JD, Soljačić M. Topological photonics. Nat Photon 2014;8:821–9.
[114] Ozawa T, Price HM, Amo A, et al. Topological photonics. Rev Mod Phys 2019;91:015006.

[115] Shima N, Aoki H. Electronic structure of super-honeycomb systems: a peculiar realization of semimetal/semiconductor classes and ferromagnetism. Phys Rev Lett 1993;71:4389–92.
[116] Lan Z, Goldman N, Öhberg P. Coexistence of spin-1/2 and spin-1 Dirac-Weyl fermions in the edge-centered honeycomb lattice. Phys Rev B 2012;85:155451.
[117] Bhattacharya A, Pal B. Flat bands and nontrivial topological properties in an extended Lieb lattice. Phys Rev B 2019;100:235145.
[118] Moulton B, Lu J, Hajndl R, Hariharan S, Zaworotko MJ. Crystal engineering of a nanoscale Kagomé lattice. Angew Chem Int Ed 2002;41:2821–4.
[119] Law K, Saxena A, Kevrekidis P, Bishop A. Localized structures in Kagome lattices. Phys Rev A 2009;79:053818.
[120] Chen Q, Bae SC, Granick S. Directed self-assembly of a colloidal Kagome lattice. Nature 2011;469:381–4.
[121] Chisnell R, Helton JS, Freedman DE, et al. Topological Magnon bands in a Kagome lattice ferromagnet. Phys Rev Lett 2015;115:147201.
[122] Kumar M, Laitinen A, Hakonen P. Unconventional fractional quantum Hall states and Wigner crystallization in suspended Corbino graphene. Nat Commun 2018;9:2776.
[123] Kollár AJ, Fitzpatrick M, Houck AA. Hyperbolic lattices in circuit quantum electrodynamics. Nature 2019;571:45–50.
[124] Zeng Y, Li JIA, Dietrich SA, et al. High-quality magnetotransport in graphene using the edge-free corbino geometry. Phys Rev Lett 2019;122:137701.
[125] Schindler F, Cook AM, Vergniory MG, et al. Higher-order topological insulators. Sci Adv 2018;4:eaat0346.
[126] Ezawa M. Higher-order topological insulators and semimetals on the breathing Kagome and pyrochlore lattices. Phys Rev Lett 2018;120:026801.
[127] Benalcazar WA, Bernevig BA, Hughes TL. Quantized electric multipole insulators. Science 2017;357:61.
[128] Fu L. Topological crystalline insulators. Phys Rev Lett 2011;106:106802.
[129] Xue H, Yang Y, Gao F, Chong Y, Zhang B. Acoustic higher-order topological insulator on a Kagome lattice. Nat Mater 2019;18:108–12.
[130] Ni X, Weiner M, Alù A, Khanikaev AB. Observation of higher-order topological acoustic states protected by generalized chiral symmetry. Nat Mater 2019;18:113–20.
[131] Peterson CW, Benalcazar WA, Hughes TL, Bahl G. A quantized microwave quadrupole insulator with topologically protected corner states. Nature 2018;555:346–50.
[132] Lim L-K, Fuchs J-N, Piéchon F, Montambaux G. Dirac points emerging from flat bands in Lieb-kagome lattices. Phys Rev B 2020;101:045131.
[133] Wang P, Zheng Y, Chen X, et al. Localization and delocalization of light in photonic moiré lattices. Nature 2019;577:42.
[134] Goblot V, Rauer B, Vicentini F, et al. Nonlinear polariton fluids in a flatband reveal discrete gap solitons. Phys Rev Lett 2019;123:113901.
[135] Jiang W, Huang H, Liu F. A Lieb-like lattice in a covalent-organic framework and its Stoner ferromagnetism. Nat Commun 2019;10:2207.